How Reducing Model Mismatch is Beneficial to EEG Source Localization: Simulation Study

Jun Hee Hong, Donghyeon Kim, and Sung Chan Jun*
School of Information and Communications,
Gwangju Institute of Science and Technology (GIST),
Gwangju, South Korea
{jun0476, danielkim, scjun}@gist.ac.kr

Abstract— **Forward modeling errors as well as measurement noise at sensor surface are propagated into errors in EEG source localization. In order to reduce forward modeling errors, tremendous effort has gone in to estimate real head models as accurately as possible, thereby, yielding more accurate source localization. Additionally, de-noising approaches have been developed to reduce the effect of noise. However, both noise and model mismatch are essentially unavoidable. Typically, the noise level depends on the EEG data to be analyzed. Unaveraged data has a substantially higher noise level than averaged data. For the given noise level of EEG data, how is reducing model mismatch beneficial to EEG source localization? In this work, we attempt to answer this question through an intensive simulation study. Three-shell (representing scalp, skull and brain) concentric spherical head models, with meshes of different fineness are generated. Assuming that the finest mesh model has no modeling errors, about 60,000 single dipole problems are generated on it. Then they are localized on several coarser models using the beamforming technique. Homogeneous conductivity values are assigned for each shell and the finite element method (FEM) is applied for forward computation. Finally, averaged localization error distribution is obtained over signal-to-noise ratios and over different mesh models to see the modeling error effects. It is found that reducing modeling errors has substantial gain in localization, but the gain is marginal after the modeling error is less than a particular value.**

Keywords: EEG, FEM, beamforming, modeling error, model mismatch, source localiztion

I. INTRODUCTION

Electroencephalography (EEG) is a non-invasive imaging technique that provides functional information in fractional milliseconds temporal resolution and thus can help one with better understanding human brain dynamics over the whole brain. In particular, EEG source localization is used to estimate neural current sources in the brain from measurement data. Inherently, source localization is mathematically ill-posed, i.e., it has no unique solution and is very sensitive to noise. For the past couple of decades, many methodologies for overcoming these difficulties have been developed [1-4]. Most source localization methods rely on forward modeling and its computation. A more accurate forward model may yield more accurate source localization. Therefore, efforts to improve forward modeling are crucial and beneficial to EEG source localization.

Source localization errors generally originate from two sources: modeling errors (such as head model mismatch and source model mismatch) and measurement noise. In order to reduce model mismatch, tremendous effort has been made in generating realistic head models incorporating inhomogeneous conductivity distribution [5, 6, therein]. Also, to reduce measurement noise, many de-noising approaches have been proposed [7, therein]. De-noising is very limited due to the nature of EEG and some noise seems essentially unavoidable. Overall, improvement of forward modeling seems to require more cost in computation and effort than de-noising.

One may develop a high resolution fine mesh head model at the expense of huge effort. It will reduce modeling errors significantly, thereby, improving source localization. However, localization errors originating from noise cannot be controlled by such efforts. Recently, single-trial EEG analysis or unaveraged EEG analysis has had more attention [8]. For those cases, EEG data are severely contaminated by noise, thus giving a substantially high noise level, therefore, a very low signal-to-noise ratio (SNR). How can such data be localized cost effectively? In other words, in the case of low SNR EEG data, is reducing model mismatch beneficial to EEG source localization?

In this study, we mainly attempt to answer these questions. Assuming that a dipole source model is as good as perfect, we are focused here on modeling errors generated from the head model mismatch. A three-shell concentric spherical model is considered here as the head model. The three shells from inner to outer represent the brain, skull and scalp layers, respectively. Each layer is assumed to have homogenous conductivity values obtained from [9]. We generated several mesh head models, each with a different resolution. For our study, we consider the finest meshed model as the modeling error-free head model, and tens of thousands singe dipole problems are generated on that model. Then, to investigate how localization errors that originate from modeling errors are distributed over a variety of SNRs, localization for all of the generated problems is performed on coarser meshed head models (with implicit modeling errors). As a localization method, the beamforming technique is applied in this work, and the finite element method (FEM) is applied for forward computation [5, 6, 10, 11].

II. METHODS

A. The EEG forward model

In a quasi-static approximation of Maxwell's equations for electric field, the distribution of electric potential V in the head Ω of conductivity σ, resulting from current source density J^p is governed by the elliptic equation as follows:

$$\nabla \cdot (\sigma \nabla V) = \nabla \cdot J^p \ \ in\ \Omega . \tag{1}$$

At the boundary of the scalp, we apply the Neumann boundary condition:

$$\sigma(\nabla V) \cdot n = 0 \ on\ \partial\Omega , \tag{2}$$

where n is the normal vector to the boundary. Using (1) and (2), a solution V satisfies

$$\int_\Omega \nabla \cdot (\sigma \nabla V) W dr = \int_\Omega W \nabla \cdot J^p dr , \tag{3}$$

where W is any differentiable function. By Green's 1st identity and boundary conditions, the following variational equation is derived:

$$\int_\Omega \sigma \nabla V \nabla W dr = \int_\Omega \nabla W \cdot J^p dr \quad \forall W . \tag{4}$$

Here, a weak solution V to (4) can be approximated by a linear combination of shape functions H_i.

$$V(r) \approx \sum_{i=1}^{N} v_i H_i(r) . \tag{5}$$

A shape function $H_i(r)$ is defined as a finite supported function having 1 at i^{th} node and 0 at other nodes.

Substituting $W(r)= H_i(r)$ and $V(r)= \sum v_i H_i(r)$ into variational equation (4) yields

$$\sum_{i,j} v_i \int_\Omega \sigma \nabla H_i \nabla H_j dr = \int_\Omega \nabla H_j \cdot J^p dr \quad \forall j . \tag{6}$$

Taking into account $\Omega = \cup_i E_i$ (E_i: element of mesh) gives

$$\sum_{i,j,k} v_i \int_{E_k} \sigma_k \nabla H_i \nabla H_j dr = \sum_k \int_{E_k} \nabla H_j \cdot J^p dr \forall j,k , \tag{7}$$

which gives linear systems of unknown v_i. This linear system can be numerically solved by the conjugate gradient (CG) method or its variants.

B. The inverse problem – Source localization

In this work, we adopted a minimum variance (MV) beamformer as the localization method. A MV beamformer is a kind of adaptive spatial filter depending on the measurement. It is reported that the MV beamformer is superior in accuracy to others [12] and, thus has been widely used in MEG/EEG source imaging [13]. In the beamforming technique, the spatial filter $\mathbf{w}(\mathbf{r})$ at $\mathbf{r}$ is applied to the measurement data, yielding the source activity at $\mathbf{r}$ as follows:

$$\hat{Q}(\mathbf{r},t) = \mathbf{w}^T(\mathbf{r})\mathbf{m}(t), \tag{8}$$

where $\hat{Q}(\mathbf{r},t)$ and $\mathbf{m}(t)$ are the estimated magnitude of the source activity at the beamforming scanning source point $\mathbf{r}$ at time t, and the spatiotemporal measurement vector at time t, respectively. Spatial filter $\mathbf{w}(\mathbf{r})$ is defined in the following optimization problem:

$$\mathbf{w}(\mathbf{r}) = \arg\min \mathbf{w}^T(\mathbf{r})\mathbf{C}\mathbf{w}(\mathbf{r}), \text{ subject to } \mathbf{w}^T(\mathbf{r})\mathbf{l}(\mathbf{r}) = 1, \tag{9}$$

where $\mathbf{C}$ is the covariance matrix of the measurement defined as $\mathbf{C} = \langle \mathbf{m}(t)\mathbf{m}^T(t) \rangle_t$ and $\langle \cdot \rangle_t$ indicates the time average. $\mathbf{l}(\mathbf{r})$ denotes a lead-field vector at the source point. This constraint minimization problem can be solved using the method of the Lagrange multiplier and explicit form of the weight spatial filter can be represented by

$$\mathbf{w}(\mathbf{r}) = \frac{\mathbf{C}^{-1}\mathbf{l}(\mathbf{r})}{\mathbf{l}^T(\mathbf{r})\mathbf{C}^{-1}\mathbf{l}(\mathbf{r})} . \tag{10}$$

Using this weight spatial filter, the time averaged source output power is obtained below:

$$\left\langle \hat{Q}(\mathbf{r},t)^2 \right\rangle_t = \mathbf{w}^T(\mathbf{r})\mathbf{C}\mathbf{w}(\mathbf{r}) = \frac{1}{\mathbf{l}^T(\mathbf{r})\mathbf{C}^{-1}\mathbf{l}(\mathbf{r})} . \tag{11}$$

When a spherical homogeneous conductor head model is introduced in forward computation, a false intensity may increase around the center of the sphere in the source imaging. To avoid this difficulty, it is known that the constraint $\mathbf{w}^T(\mathbf{r})\mathbf{l}(\mathbf{r}) = \|\mathbf{l}(\mathbf{r})\|$ in place of $\mathbf{w}^T(\mathbf{r})\mathbf{l}(\mathbf{r}) = 1$ is applied [9]. This is called an array-gain MV beamformer. Its output power is expressed as

$$\left\langle \hat{Q}(\mathbf{r},t)^2 \right\rangle_t = \frac{1}{\tilde{\mathbf{l}}^T(\mathbf{r})\mathbf{C}^{-1}\tilde{\mathbf{l}}(\mathbf{r})} = \frac{\mathbf{l}^T(\mathbf{r})\mathbf{l}(\mathbf{r})}{\mathbf{l}^T(\mathbf{r})\mathbf{C}^{-1}\mathbf{l}(\mathbf{r})} . \tag{12}$$

The vector type beamformer can be defined by weight matrix $\mathbf{W}(\mathbf{r}) = [\mathbf{w}_x(\mathbf{r}), \mathbf{w}_y(\mathbf{r}), \mathbf{w}_z(\mathbf{r})]$. The output power of the array-gain vector type beamformer is expressed as:

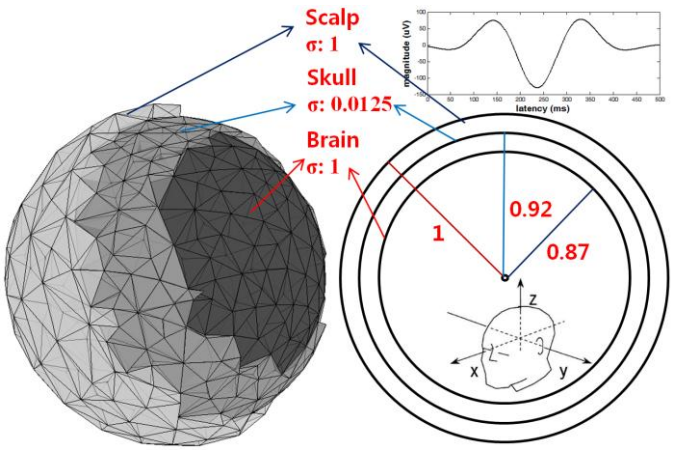

Fig. 1. Example of a three layer volume meshed spherical head model (left), representing layer information of radii ratio and conductivity (right), and time course of dipole source used for numerical simulations (top right).

$$\left\langle \hat{Q}(\mathbf{r},t)^2 \right\rangle_t = \|\mathbf{l}(\mathbf{r})\|^2 \left[\mathbf{L}^T(\mathbf{r})\mathbf{C}^{-1}\mathbf{L}(\mathbf{r})\right]^{-1}. \quad (13)$$

III. Experiments and Results

Forward and inverse computations based on formulations in Section 2 were implemented in the Matlab computing language. In order to reduce computation time and use memory resources efficiently, we adopted the technical algorithm in [14] rather than the conventional 'for' routine algorithm when the global system matrix in the FEM analysis is generated. In short, this algorithm uses a sparse matrix for efficient memory resource use and indexing the matrix technically. Further, when the element index is sought in containing the given source(s) or electrode(s), normal vectors on each tetrahedron face are used. To speed up computation, all pre-computable data were saved and properly loaded at use. As a FEM solver, the biconjugate gradient stabilized method is used, which is good at solving a large and sparse system of linear equations (global system matrix). To verify our computation, both the Zhang [9] and Yao [15] analytic solution forward models were implemented for comparison. As addressed in Section 2, an array-gain vector type beamformer is applied for localization. A dipole source is determined to be located where maximum output power occurs.

A. Configuration for Simulations

Numerical experiments were conducted on a workstation (Intel Xeon 2 Quadcore CPU at 3GHz, 64bit OS and 24GB RAM). A three-shell concentric spherical mesh head model was generated with brain, skull and scalp having proper conductivity values (i.e., within each layer of tetrahedrons, the conductivity values are uniform) on each layer (Fig. 1). In this work, six mesh head models were constructed as follows (Fig. 2):

Mesh 1: 2,455 tetrahedrons and 471 vertices
Mesh 2: 5,637 tetrahedrons and 1,057 vertices
Mesh 3: 19,834 tetrahedrons and 3,646 vertices
Mesh 4: 30,242 tetrahedrons and 5,535 vertices
Mesh 5: 64,089 tetrahedrons and 11,575 vertices
Mesh 6: 113,255 tetrahedrons and 21,798 vertices.

Among them, the finest model (Mesh 6) was chosen as a head model with no modeling errors. The radius of outer layer (scalp) is set to 10cm, and radii of other layers are determined proportionally, as illustrated in Fig. 1. Here 32-sensor array geometry of the LAXTHA WEEG-32 EEG system is used.

Dipole sources were generated to be located above z=1 plane (x-y plane) and within the inner shell (brain layer). Synthetic data was generated by adding white Gaussian noise to sensor values computed through the forward model. A total of 1,000 randomly distributed dipole sources at random orientations were generated for synthetic measurements. A synthetic electric field with a temporal window of 500 time points was generated with a damping sinusoidal time course for each dipole (Fig. 1). For each dipole, five different noise realizations and 12 different SNRs (between -14dB and 8dB) were generated by controlling the noise power. Here SNR is defined by

$$\text{SNR (dB)} = 10\log_{10}(\|\mathbf{S}\|_F^2 / \|\mathbf{N}\|_F^2),$$

where **S** and **N** are the signal and noise matrices, respectively, and $\|\cdot\|_F$ is a Frobenius norm. Thus, a total of 60,000 single dipole problems were tested to do source localization through the beamforming technique. A full beamforming scan requires 156,271 scans (2 mm scanning resolution) for one localization. To speed-up source localization, lead-field vectors at predetermined scanning points in the head were pre-computed.

B. Localization Error Distribution over SNRs and over Modeling Errors

Coarser meshes implicitly have modeling errors with relative magnitude. The extent of the mismatch between a corresponding mesh and the modeling-error-free mesh (Mesh 6) represents the magnitude of modeling errors. Therefore, Mesh 1 and Mesh 5 have the largest and smallest modeling errors, respectively, and Mesh 2, Mesh 3 and Mesh 4 are in the middle.

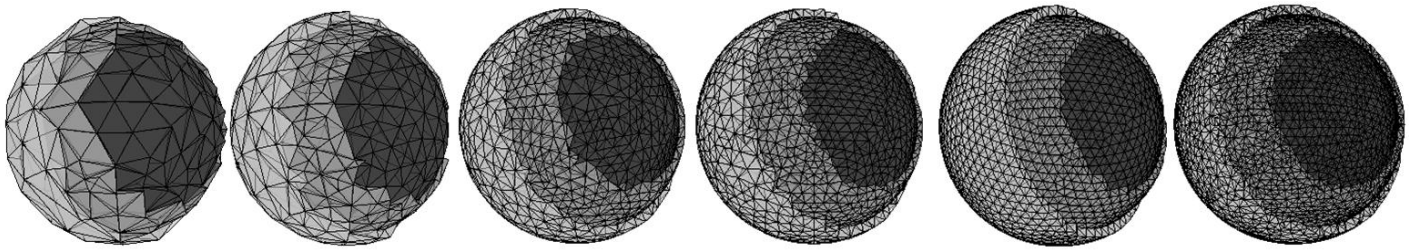

Fig. 2. Six kinds of meshed head model. Rightmost model is assumed as the head model without modeling error.

For each mesh, 60,000 single dipole problems were tested to yield localization error distribution over SNRs. Fig. 3 shows the localization error distributions over SNRs of the 6 meshes.

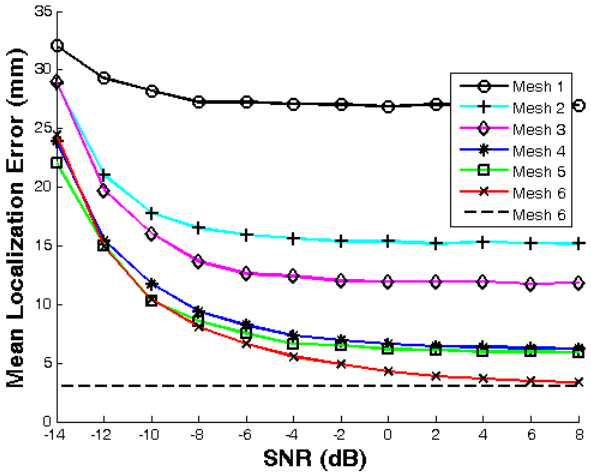

Fig. 3. Mean localization error over various SNRs. Each mark (or color) represents the mesh head model. The dotted line represents averaged localization error for noise-free data (essential spatial resolution of beamforming technique).

As we expected, localization errors gets larger as the SNR gets lower, regardless of mesh fineness. We note that the dotted line represents the canonical localization error (3.055 mm) induced by the beamforming technique (2 mm scanning resolution). This canonical localization error was estimated from localization results of 1,000 noise-free single dipole problems. In general, localization errors are composed of errors from modeling mismatch and errors from noise. In Fig. 3, the red line represents the sum of the beamforming canonical errors and localization errors originating from noise only, because Mesh 6 was assumed to have no model mismatch. Therefore, localization errors originating from modeling mismatch can be roughly estimated by subtracting the result of Mesh 6 from the results of the other meshes, which is shown in Fig. 4. In Fig. 4, negative values were set to zero since they are meaningless.

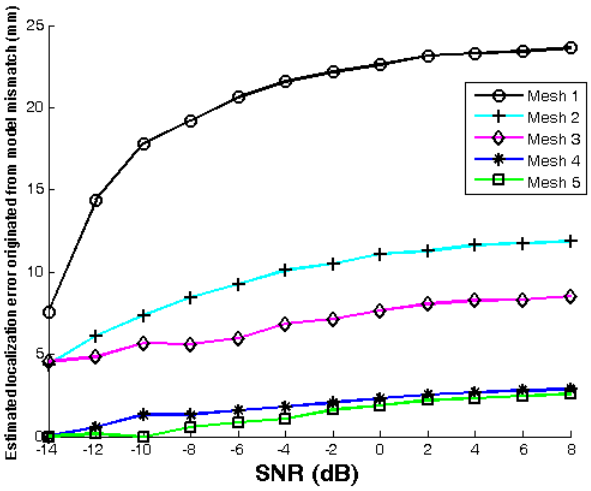

Fig. 4. Mean localization error originated from model mismatch over various SNRs.

As the modeling errors are reduced, that is, the mesh model gets finer and closer to Mesh 6, localization errors originating from model mismatch decrease significantly around the high or middle SNR ranges, while it goes to some marginal values for very low SNRs. Interestingly, Mesh 4 and Mesh 5 have negligible model mismatch effect on localization for very low SNRs, and Meshes 2 and 3 have no difference for low SNRs. From Fig. 4, we can infer how a fine mesh head model is used in an efficient manner for the given SNR range. In localizing a EEG data with heavy noise, a fine mesh is not efficient, but a coarser model could be a more cost-effective choice.

IV. Discussion

Assuming the finest mesh head model is considered as the base model (a perfect model with no model mismatch), we have investigated how localization errors are distributed over SNRs and over the extent of model mismatch. We have roughly estimated localization errors originating from model mismatch. We found that the model mismatch effect on localization was diminished as the SNR gets lower. For very low SNRs, the effect becomes negligible, thus improvement on modeling may be of no gain in terms of efficacy.

In this work, for simplicity, a multi-shell concentric spherical head model was used. Study with a realistic head shaped model considering inhomogeneity or moderate variation of conductivity will give a sounder conclusion.

The beamforming technique has a disadvantage in that the spatial resolution possibly relies on the scanning resolution, thus other localization methods may be applicable. However, we expect that it has minimal influence on the results.

Acknowledgments

This work is supported by NRF-2009-0071225, NIPA-2011-C1090-1131-0006, and the BioImaging Research Center at GIST.

References

[1] M. Hämäläinen, R. Hari, R. J. Ilmoniemi, J. Knuutila, and O. V. Lounasmaa, "Magnetoencephalography---theory, instrumentation, and applications to noninvasive studies of the working human brain," Rev. Mod. Phys., vol. 65, pp. 413-497, 1993.

[2] S. Baillet, J. C. Mosher, and R. M. Leahy, "Electromagnetic Brain Mapping," IEEE Signal Processing Magazine, vol. 18, pp. 14-30, 2001.

[3] S. C. Jun, B. A. Pearlmutter, and G. Nolte, "Fast accurate MEG source localization using a multilayer perceptron trained with real brain noise," Phys. Med. Biol., vol. 47, pp. 2547–2560, 2002.

[4] S. C. Jun, J. S. George, J. Pare-Blagoev, S. M. Plis, D. M. Ranken, D. M. Schmidt, and C. C. Wood, "Spatiotemporal Bayesian inference dipole analysis for MEG neuroimaging data," NeuroImage, vol. 28, pp. 84-98, 2005.

[5] C. H. Wolters, A. Anwander, X. Tricoche, D. Weinstein, M. A. Koch, and R. S. MacLeod, "Influence of tissue conductivity anisotropy on EEG/MEG field and return current computation in a realistic head model: A simulaion and visualization study using high-resolution finite element modeling," NeuroImage, vol. 30, pp. 813-826, 2006.

[6] C. H. Wolters, "The Finite Element Method in EEG/MEG Source Analysis," SIAM News, vol. 40, pp. 1-2, 2007.

[7] T. P. Jung, S.Makeig, M. J. Mckeown, A. J. Bell, T-W. Lee, and T. J. Sejnowski, "Imaging Brain Dynamics Using Independent Component Analysis," Proc. IEEE, vol. 89, pp. 1107-1122, 2001.

[8] B. Blankertz, R. Tomioka, S. Lemm, M. Kawanabe, and K-R. Müller, "Optimizing Spatial Filters for Robust EEG Single-Trial Analysis." IEEE Signal Processing Magazine, vol. 25, pp. 41-56, 2008.

[9] Z. Zhang, "A Fast Method to Compute Surface Potentials Generated by Dipoles within Multilayer Anisotropic Spheres," Phys. Med. Biol., vol. 40, pp. 335-349, 1995.

[10] Y. Yan, P. L. Nunez, and R. T. Hart, "Finite-element model of the human head: scalp potentials due to dipole sources," Med. & Biol. Engineering & Computing, vol. 29, pp. 475–481, 1991.

[11] R. Rytsar, and T. Pun, "Computational aspects of the EEG forward problem solution for real head model using finite element method," Proceedings of the 29th Annual International conference of the IEEE EMBS, pp. 829-832, 2007.

[12] K. Sekihara, M. Sahani, and S. S. Nagarajan, "Location bias and spatial resolution of adaptive and non-adaptive spatial filters for MEG source reconstruction," NeuroImage, vol. 25, pp. 1056-1067, 2005.

[13] K. Sekihara, and S. S. Nagarajan, "Adaptive Spatial Filters for Electromagnetic Brain Imaging," Springer, 2008.

[14] A. Ortiz, "On efficient finite element assembly in Matlab," [Online] Available: http://www.imechanica.org/node/7552, 2010.

[15] D. Yao, "Electric potential produced by a dipole in a homogeneous conducting sphere," IEEE Trans. Biomed. Eng., vol. 47, pp. 964-966, 2000.